Available online at www.sciencedirect.com
SCIENCE DIRECT
Computers and Electronics in Agriculture 52 (2006) 107–118
Computers and electronics in agriculture
www.elsevier.com/locate/compag

Sensor-in-the-loop tractor stability control: Look-ahead attitude prediction and field tests

M. Kise, Q. Zhang *

Department of Agricultural and Biological Engineering, University of Illinois at Urbana-Champaign, 1304 W. Pennsylvania Ave., Urbana, IL 61801, USA

Received 3 May 2005; received in revised form 8 February 2006; accepted 14 February 2006

Abstract

Rollover protective structures (ROPS) have been recognized as the most effective device to prevent tractor-related fatalities due to tractor rollover. However, ROPS provide only passive protection from rollover-caused fatalities. The most effective way to eliminate rollover-caused fatalities is to prevent the rollover from occurring. This research proposes the use of "sensor-in-the-loop (SIL)" online tractor attitude and motion simulation to provide rollover warnings based on estimated look-ahead tractor attitude and motion status. A stereovision camera was used as the visual sensor for the SIL system to create a three-dimensional virtual terrain map on which a virtual vehicle travels. This progressively estimates the tractor attitude and motion on the terrain to provide warning of potential rollovers. A series of field tests on various terrains were conducted to evaluate the dynamic performance of the SIL tractor motion simulator in an actual field environment. The validation test results indicated that the SIL vehicle attitude simulator could predict the attitude and motion status of the vehicle approximately 8.0 m ahead of its actual position with favorable and consistent accuracy at all test sites. Such information can be used as baseline data for a warning signal to prevent rollovers from occurring.

Keywords: Tractor rollover; Roll and pitch; Stereovision; Vehicle motion simulation; 3D terrain map

1. Introduction

Agricultural mechanization was one of the most significant achievements of engineering in the 20th century. While mechanization greatly helps farmers achieve highly efficient production, it also creates a hazardous work environment for them. The statistics on occupational fatal accidents indicate that farms are considered one of the most hazardous work environments in the United States (Personick and Windau, 1997; National Safety Council, 1999). Historical data shows the fatality rate in agriculture remained about 22/100,000 workers through the 1990s, while tractor-related accidents cause approximately 300 fatalities each year (Rautiainen and Reynolds, 2002). Tractor rollovers cause over 50% of fatalities from agricultural accidents each year (Hard et al., 1999). Even with enormous efforts to improve tractor safety designs, the rate of tractor-related fatalities has shown a slight increase mainly due to the inadequate maneuvering of the tractor (Myers et al., 1998).

Rollover protective structures (ROPS) have been one of the most important advances in protecting the driver from tractor overturn accidents (ASAE, 1997). However, more than 40% of existing tractors are not equipped with an ROPS

* Corresponding author. Tel.: +1 217 333 9419; fax: +1 217 244 0323.
E-mail address: qinzhang@uiuc.edu (Q. Zhang).

0168-1699/$ – see front matter © 2006 Elsevier B.V. All rights reserved.
doi:10.1016/j.compag.2006.02.003

device (Wilkins et al., 2003). Some specific farming tasks do not allow tractors to be equipped with an ROPS. For example, the low-clearance of fruit trees in an orchard prevents tractors from being equipped with an ROPS in order to travel freely between the trees. To provide necessary protection to drivers working in such a confined environment, researchers have created automatically deployed ROPS systems. These systems could retract in a stable status and be deployed when an unstable traveling status was detected (Powers et al., 2001; Etherton et al., 2002a, 2002b).

It is important to point out that ROPS provides only passive protection to reduce rollover-caused fatalities. The most effective way to eliminate rollover-caused fatalities is the prevention of rollover occurrences. One possible means of preventing tractor rollovers is to better understand the cause of a tractor rollover under various traveling conditions and to improve the tractor stability under such conditions. To investigate tractor stabilities under various traveling conditions, Davis and Rehkugler (1974a,b) conducted a scale-model study of wheel-tractor overturns by utilizing a physical scale-model tractor in the verification of a mathematical model for tractor overturning motions. Similarly, Liu and Ayers (1998, 1999) have conducted tractor stability tests using radio-controlled tractors to study the effects of tractor dynamic state variables, such as the roll and pitch angles or rates on the tractor stability at terrains with different slopes.

The research described in this paper used a "sensor-in-the-loop (SIL)" vehicle attitude simulator to perform an on-line prediction of the vehicle attitude and motion as baseline data while the vehicle was traveling on the detected terrain under detected motion status. This SIL simulator uses a vehicle-mounted stereovision camera to detect the immediate terrain in front of the moving vehicle, and then uses this terrain information to create a 3D terrain map on which a virtual vehicle will travel to estimate the future roll and pitch angles and/or rates of the moving vehicle on the terrain. The estimated vehicle attitude and motion parameters are dominant factors for assessing tractor rollover potential and therefore provide the baseline information for a tractor rollover warning. The following sections introduce the methodology developed in this research in detail.

2. SIL vehicle attitude and motion simulator

2.1. Stereovision system

As described previously, the SIL vehicle attitude simulator is based on a 3D terrain map created from the 3D terrain images taken using a vehicle-mount stereovision camera. The stereovision camera consists of two identical cameras geometrically arranged parallel to each other. A stereovision image of a field scene is generated using two plane images simultaneously taken using these two cameras as illustrated in Fig. 1. A 3D image can be reconstructed based on the difference between the two plane images of the same scene, and therefore is less sensitive to ambient light changes (Reid and Searcy, 1987). A few successful applications using a stereovision system have been recently reported. Some applications in agriculture include guiding a tractor within crop rows (Kise et al., 2005), creation of 3D crop maps

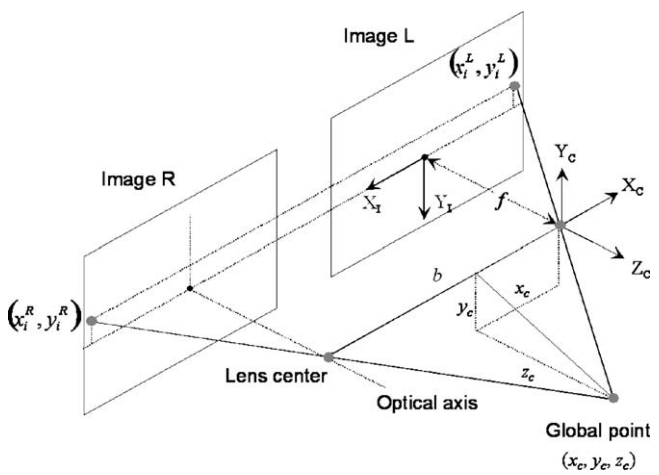

Fig. 1. Geometric relation ship of stereovision system.

based on aerial stereo images (Rovira Más et al., 2005), estimating physical parameters of a transplant in plug tray (He et al., 2003), estimating the mass of swimming fish (Lines et al., 2001), and extracting the 3D shape of live pigs (Wu et al., 2004).

To interpret the information carried in a stereo image, it is important to know how that image is constructed. The original stereo image is carried using two separate plane images denoted image L and image R, as shown in Fig. 1. The distance between the centers of the two lenses is defined as the baseline b, and the focal length of the lens pair is defined as f. It should be noted that the projection on the image plane is a reverse of the scene due to the pinhole camera model geometry. Assuming both plane images are laid on the same plane and their horizontal axes are aligned, the location of an identified pixel ($X_I Y_I$ coordinates) can be defined as $\left(x_i^L, y_i^L\right)$ in image L and as $\left(x_i^R, y_i^R\right)$ in image R.

In terms of the location difference of the projections of an object of interest in the left and right plane images, the distance of the object to the center of the stereo camera lens, z_c, can be calculated using the following equation based on the image pixel distances x_i^L and x_i^R:

$$d = x_i^L - x_i^R = \frac{bf}{rz_c} \tag{1}$$

where r is the distance between pixels.

In Eq. (1), the variable d can be defined as the disparity of a point in a stereo image. Since the disparity of a point is inversely proportional to its depth, the disparity image provides a direct (but inverse) encoding of the scene depth (Scharstein, 1999). Once the disparity image is obtained, the 3D location of a point (x_c, y_c, z_c) in the left camera coordinates can be determined as follows:

$$x_c = \frac{x_i^L}{f} z_c = P\frac{x_i^L}{d}, \qquad y_c = P\frac{y_i^L}{d}, \qquad z_c = P\frac{f}{d} \tag{2}$$

where $P = (b/r)$ is a constant of the digital stereo camera.

2.2. Vehicle platform

To support SIL vehicle rollover precaution technology research, a research vehicle platform has been developed based on a John Deere agricultural utility vehicle. As shown in Fig. 2, the stereovision camera is installed on the research vehicle platform. The stereo camera is installed on a sensor frame 2.2 m above ground level in front of the vehicle platform. The camera mount is configured to be capable of obtaining the field of view containing a 1.2 m (width) × 3.7 m (length) rectangle located about 5.0 m ahead of the vehicle as the region of interest (ROI). The 3D terrain map is created to represent this ROI. The camera configuration is defined by six parameters: camera mounting angles of tilt σ_x, pan σ_y and roll σ_z, and camera position offset (x_d, y_d, z_d) to the vehicle center of gravity (CG). These parameters were 33°, 3° and 0° for tilt, pan and roll angles, and 1.00, 0.05 and 2.20 m for x_d, y_d and z_d, respectively on the research vehicle platform.

Besides the stereovision camera, the vehicle platform is also equipped with an inertial measurement unit (IMU, JCS-7401A, JAE, Tokyo, Japan) to measure the actual vehicle attitude and motion as the reference signal. This is used to evaluate the accuracy of the simulation results. This IMU consists of three fiber optical gyroscopes and three acceleration sensors. Both gyroscopes and accelerometers are geometrically arranged perpendicular to each other, and can measure roll and pitch angles and/or angular rates of the vehicle platform dynamically with an accuracy of ±2° for the angles, and ±5° s^{-1} for the angular rates. The roll and pitch angles are used for the 3D terrain map creation.

2.3. SIL vehicle attitude simulator

One of the dominant factors causing a tractor rollover is how a tractor travels on a slope. The attitude of a tractor on a slope is expressed by roll and pitch angles, and a stationary tractor's static equilibrium determines whether it will overturn on the slope. For a more reliable prediction of a tractor rollover, the dynamic motion of the vehicle, namely the roll and pitch angular rates, need to be considered. In this research, the attitude and motion of a tractor is simulated as it travels on a virtual 3D map created by acquired 3D terrain images using the vehicle-mounted stereovision camera.

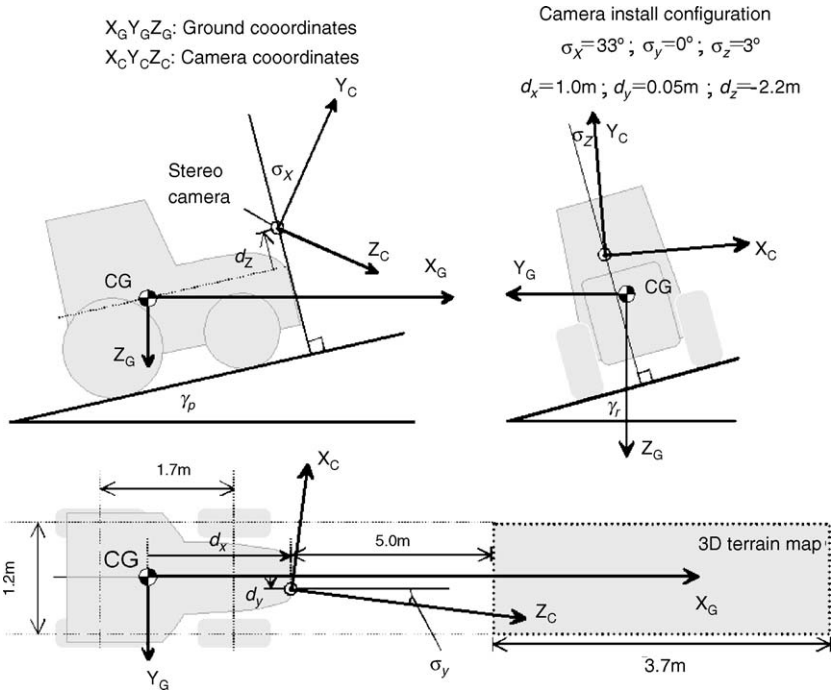

Fig. 2. Coordinate systems and physical specification of the platform vehicle; camera install configuration and geometric relationship between the ground coordinates, the camera coordinates and 3D terrain map.

Fig. 3 shows the information flowchart of the SIL tractor motion simulator. This consists of the field scene stereo image acquisition, 3D terrain map creation, and vehicle motion simulation. Among them, the creation of the 3D terrain map plays the key role in this SIL simulation. This 3D terrain map creation reconstructs a virtual 3D field terrain located in front of the vehicle based on the acquired 3D field scene images. The 3D map provides the base for estimating the roll and pitch angles of the vehicle. The roll and pitch angular rates can then be calculated in terms of a series of estimated roll and pitch angles by means of the numerical differentiation method of the five-point rule derived from the Lagrange interpolating polynomial (Yakowitz and Szidarovszky, 1989), described below.

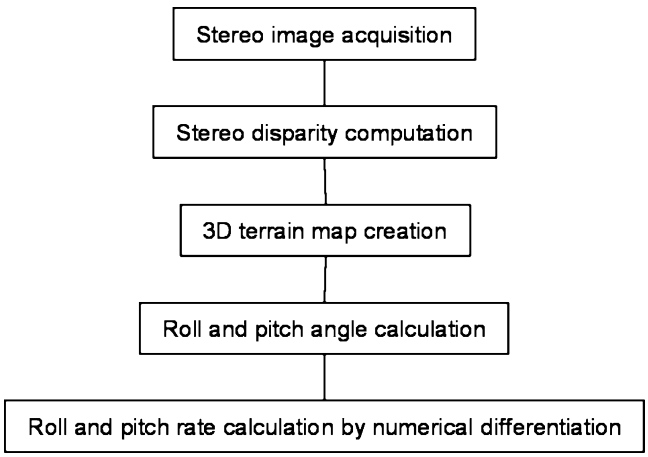

Fig. 3. Step-by-step procedure for online vehicle motion simulation.

2.4. Reconstruction of a 3D terrain map

The 3D terrain map (also called the virtual field) creation is a fundamental part of this SIL vehicle attitude simulator. Vehicle motion, described by vehicle roll and pitch as well as their angular rates, is simulated as a hypothetical vehicle travels on a reconstructed virtual 3D terrain map. This 3D terrain map should represent not only the slope of the field terrain the vehicle will travel on, but also irregularities of the terrain surface in order to determine the vehicle attitude and motion dynamics comprehensively and accurately.

The ground coordinates $X_g Y_g Z_g$ of the virtual field is defined by setting its origin at the vehicle CG as shown in Fig. 2. The X_g and Y_g axes of the ground coordinates are defined as the longitudinal and lateral directions of the vehicle, respectively, and the Z_g axis is parallel to the gravity direction. Similarly, the camera coordinates $X_c Y_c Z_c$ are defined by setting its origin at the center of the left camera focal point, with its X, Y and Z axis arbitrarily defined as shown in Fig. 2. To create a 3D virtual field and to represent the slope and irregularities of the field terrain ahead of the vehicle, it is necessary to convert the locations of 3D points in the stereo image from the camera coordinates into the ground coordinates. This transformation is expressed as follows (Beggs, 1983):

$$\begin{pmatrix} x_g \\ y_g \\ z_g \end{pmatrix} = \begin{pmatrix} 0 & 0 & 1 \\ -1 & 0 & 0 \\ 0 & -1 & 0 \end{pmatrix} R_Y(\sigma_y) R_X(\sigma_x - \gamma_p) R_Z(\sigma_z - \gamma_r) \begin{pmatrix} x_c \\ y_c \\ z_c \end{pmatrix} + \begin{pmatrix} x_d \\ y_d \\ z_d \end{pmatrix} \tag{3}$$

where σ_x, σ_y, and σ_z are the tilt, pan and roll angles of the camera mount, (x_d, y_d, z_d) is the camera position offset to the tractor CG.

Because stereovision systems can only create a terrain with respect to the platform vehicle, the roll and pitch angles of the platform have to be provided to create 3D terrain with respect to the ground coordinates. The IMU was installed on the platform and measured the roll angle γ_r, and pitch angle γ_p of the vehicle. R_X, R_Y and R_Z are rotation matrices around X_c, Y_c, and Z_c axes as defined below:

$$R_X(\theta) = \begin{pmatrix} 1 & 0 & 0 \\ 0 & \cos\theta & \sin\theta \\ 0 & -\sin\theta & \cos\theta \end{pmatrix}$$

$$R_Y(\theta) = \begin{pmatrix} \cos\theta & 0 & -\sin\theta \\ 0 & 1 & 0 \\ \sin\theta & 0 & \cos\theta \end{pmatrix}$$

$$R_Z(\theta) = \begin{pmatrix} \cos\theta & \sin\theta & 0 \\ -\sin\theta & \cos\theta & 0 \\ 0 & 0 & 1 \end{pmatrix}$$

where θ is a rotational angle. The 3D virtual field is formed as a matrix with each element representing the elevation of corresponding locations. This virtual field is configured as 1.2 m × 3.7 m rectangular space, with a resolution of 0.02 m × 0.02 m which results in a 60 × 185 matrix to form the virtual field. This virtual field will provide a space large enough for the virtual vehicle to travel a distance of 2.0 m to demonstrate the methodology.

2.5. SIL vehicle motion simulation

2.5.1. Roll and pitch angle estimation

Once the 3D virtual field is created from a stereo image, a look-ahead location of the vehicle in the field terrain is given by placing a virtual vehicle on the virtual field. The virtual vehicle is placed on the virtual terrain as the CG of the vehicle is located directly over the center of the map (Fig. 4).

The plane on which the vehicle is being placed can be expressed by the following equation:

$$a_p x_g + b_p y_g + c_p z_g + 1 = 0 \tag{4}$$

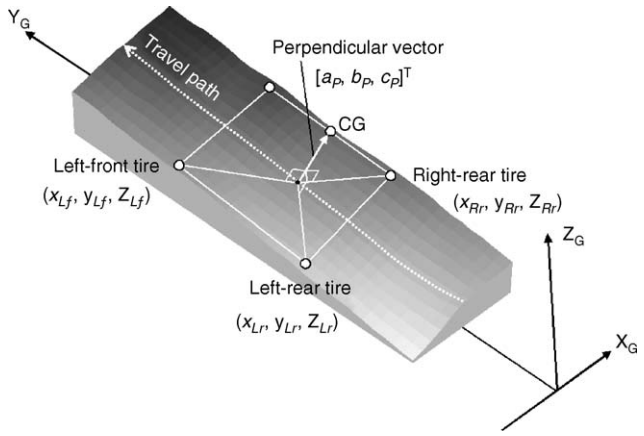

Fig. 4. 3D terrain map and hypothetical location of the vehicle: roll and pitch angles are calculated by placing a virtual vehicle on the center of the map; in order to calculate roll and pitch rates, the virtual vehicle travels on the map along to the longitudinal direction.

where $[a_p, b_p, c_p]^T$ is the vector perpendicular to the plane, and hence represents the attitude of the vehicle. This vector can be identified by substituting the tire positions of a virtual vehicle into Eq. (4):

$$\begin{pmatrix} x_{Lf} & y_{Lf} & z_{Lf} \\ x_{Lr} & y_{Lr} & z_{Lr} \\ x_{Rr} & y_{Rr} & z_{Rr} \end{pmatrix} \begin{pmatrix} a_p \\ b_p \\ c_p \end{pmatrix} - \begin{pmatrix} 1 \\ 1 \\ 1 \end{pmatrix} = 0 \tag{5}$$

where (x_{Lr}, y_{Lr}, z_{Lr}), (x_{Lf}, y_{Lf}, z_{Lf}) and (x_{Rr}, y_{Rr}, z_{Rr}) are the locations of the tire-ground contact patch on the map for left-rear, left-front and right-rear tires, respectively.

Since the number of unknowns in Eq. (4) is three, three tire locations are sufficient to solve these unknown parameters. The locations of three tires are determined from the location of the vehicle CG with respect to the virtual field and the physical dimension of the vehicle platform under the assumption that the vehicle travels in parallel to the longitudinal direction of the virtual field.

Because $[a_p, b_p, c_p]^T$ is perpendicular to the plane on which the vehicle is traveling, this vector can be defined as the gravitational vector that rotates θ_r around the X_g axis first, then rotates θ_p around the Y_g axis. θ_r and θ_p are defined as the pitch and roll angles of the virtual vehicle on the field terrain, and therefore, can be represented by the following equation:

$$R_Y(-\theta_p)R_X(-\theta_r) \begin{pmatrix} 0 \\ 0 \\ h \end{pmatrix} = \begin{pmatrix} a_p \\ b_p \\ c_p \end{pmatrix} \tag{6}$$

where $h = \sqrt{a_p^2 + b_p^2 + c_p^2}$.

From Eq. (6), the following relationships can be obtained:

$$\sin\theta_p \cos\theta_r h = a_p, \qquad -\sin\theta_r h = b_p, \qquad \cos\theta_r \cos\theta_p h = b_p \tag{7}$$

The above relationships define the roll and pitch angles:

$$\theta_r = -\sin^{-1}\left(\frac{b_p}{h}\right) \tag{8}$$

$$\theta_p = \tan^{-1}\left(\frac{a_p}{b_p}\right) \tag{9}$$

2.5.2. Roll and pitch rates estimation

It is important for tractor rollover prediction to take the disturbances of motion into consideration. Such disturbances normally arise from irregularities on the field surface and tend to overturn the tractor (Spencer and Gilfillan, 1976).

Ground irregularities are directly transferred into a moving vehicle through tire-ground contact patches and generate irregular rolling and pitching motions on the vehicle. The roll and pitch rates excite the kinetic energy of the moving vehicle that contributes to the loss of stability in vehicle motion. The purpose of the vehicle attitude simulator in this research is to predict a vehicle motion status, including the roll and pitch angles and/or angular rates for designing a tractor rollover prediction system.

In representation of the roll and pitch rates of a moving vehicle, it is practicable to assume a Gaussian process for the roll and pitch angular rates estimation (Spencer and Gilfillan, 1976). A Gaussian process is characterized by the average and standard deviation. Therefore, the roll and pitch rates of the virtual tractor are estimated using the average and standard deviation calculated from the data series obtained in a time window at the vehicle attitude simulator. This method of representation implies some practical advantages in the design of a tractor rollover prediction model. To determine the allowable roll/pitch rates to prevent the rollover, it is not necessary to consider the variation of a value if that value is large relative to the standard deviation because the probability of such a roll or pitch rate is very small. For example, if the variation is three times the standard deviation (3σ) the probability is less than 0.27%. Therefore, the rollover prediction system needs only to assess the possibility of rollover for a roll rate variation range between $-4.0^\circ\,s^{-1}$ and $5.0^\circ\,s^{-1}$ when the average roll rate is $0.5^\circ\,s^{-1}$ with a $1.5^\circ\,s^{-1}$ standard deviation with a 3σ norm.

To calculate roll and pitch rates of the vehicle on a 3D virtual field, a numerical differentiation method of the five-point rule is used (Yakowitz and Szidarovszky, 1989). This five-point rule is derived from the Lagrange interpolating polynomial. Roll and pitch rates calculated from the five-point rule in this research are expressed as follows:

$$\dot{f}_t = \frac{v_t}{12\delta}(f_{t-2} - 8f_{t-1} + 8f_{t+1} - f_{t+2}) \tag{10}$$

where f_t is the data series that has to be differentiated, namely the roll or pitch angle. In this specific case, v_t is a forward speed, and δ is the resolution of the 3D map (2 cm in this case). As suggested by its name, the first derivative is calculated based on the five points around the point f_t.

In order to obtain the average and standard deviation of the roll and pitch rates, a series of roll and pitch rates data should be calculated in the SIL vehicle motion simulation. Specifically, in this demonstration simulation, the set of roll and pitch angles were calculated as the virtual vehicle traveled on the 3D virtual field for 2.0 m along the longitudinal direction as shown in Fig. 4. The roll and pitch rates data series were calculated using the five-point rule as describe earlier.

3. Results and discussion

3.1. Static tests

A static test was conducted to evaluate a baseline performance of the SIL vehicle attitude simulator. A flat wooden board was placed in various attitudes in front of the stationary vehicle platform as imitative slopes. To perform the static test, a 1.2 m × 2.4 m wooden board was placed 5.0 m ahead of the vehicle with eight different attitudes in pitch direction from 0° to 70° with a 10° increment. One of the test settings for the static test on which the board was set at a 30° pitch angle (Fig. 5). A 3D virtual slope map was reconstructed from the acquired stereo image. In this stereo image, the white regions of the board (indicated by the white quadrangle) were used for the stereo computation to reconstruct the 3D virtual slope map. An approximate plane in terms of the least squares norm was calculated to represent the roll and pitch angles of a virtual vehicle while placed on the slope.

The results obtained from the static test are summarized in Table 1. The roll and pitch angles of the board at each attitude were measured using the IMU as the reference. The accuracy of the 3D slope reconstruction was quantitatively evaluated by calculating the errors, namely the differences between the calculated and the measured roll and pitch angles of the board, for all test conditions. The result obtained from the static test verified that it is feasible to accurately reconstruct field slopes in a 3D virtual space based on stereovision images of the field scenes. The reconstruction accuracy was better than 3.0° for both roll and pitch angles. The RMS errors of the roll and pitch angle reconstruction were 1.4° and 2.2°, respectively.

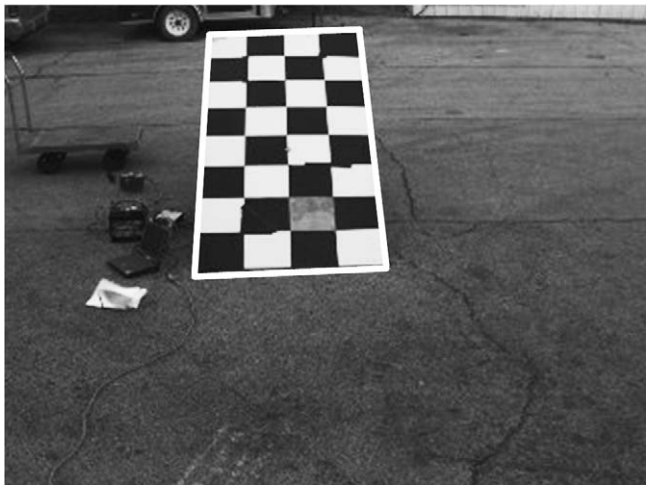

Fig. 5. Original image taken by left camera in the static test when the board is set at 30° of pitch angle. The region indicated by white quadrangle is used as ROI of the 3D space.

3.2. Dynamic tests

A series of field tests on various terrains were conducted to evaluate a dynamic performance of the SIL vehicle attitude simulator in an actual field environment. The motion simulator was installed on the research vehicle platform and was used to dynamically predict the attitude and motion of the vehicle while the vehicle was traveling in the field on a predetermined straight path at a constant speed (1.2 m/s). These dynamic field tests were conducted on a grassy hill at the University of Illinois at Urbana-Champaign Campus. This test site consists of several small hills with various slopes. During the test, stereo images of the field terrain from the view point on the moving vehicle were acquired to support the reconstruction of the virtual field. Creation of a 3D virtual field based on an acquired stereo image from the test site is illustrated in Fig. 6. In this example, the pair of original images of the field scene was taken by the vehicle-mounted stereo camera while the vehicle was traveling on a side bank on the test site. The white quadrangle in the original left image (Fig. 6(a)) indicates the ROI of the 3D terrain map as shown in Fig. 6(d). The 3D virtual field was reconstructed using the 3D information provided by the disparity image, computed from the acquired stereo image, of the field scene (Fig. 6(c)).

The elevation contour of the test path on which the vehicle traveled to perform the dynamic test is shown in Fig. 7. The elevation contour data was measured using an RTK-GPS installed on the platform vehicle. As shown in the figure, this particular path has a 5.2 m elevation difference with both up-hill and down-hill slopes. Fig. 8 compares the roll angle predicted by the motion simulator with the reference values measured using the IMU when the vehicle platform

Table 1
Result of the static test: eight different slopes in pitch direction from 0° to 70° in 10° step are reconstructed in 3D field scene by stereovision

Slope (°)		Error (°)	
Pitch	Roll	Roll	Pitch
1.9	0.9	0.5	0.1
13.7	2.1	−2.3	0.7
24.3	2.3	−3.0	−0.5
29.5	2.4	2.8	−1.2
40.8	0.3	1.1	0.0
53.8	2.3	−2.7	−2.5
62.3	−0.2	−1.6	2.0
71.3	−0.2	−1.5	0.9
RMS error		1.3	2.1

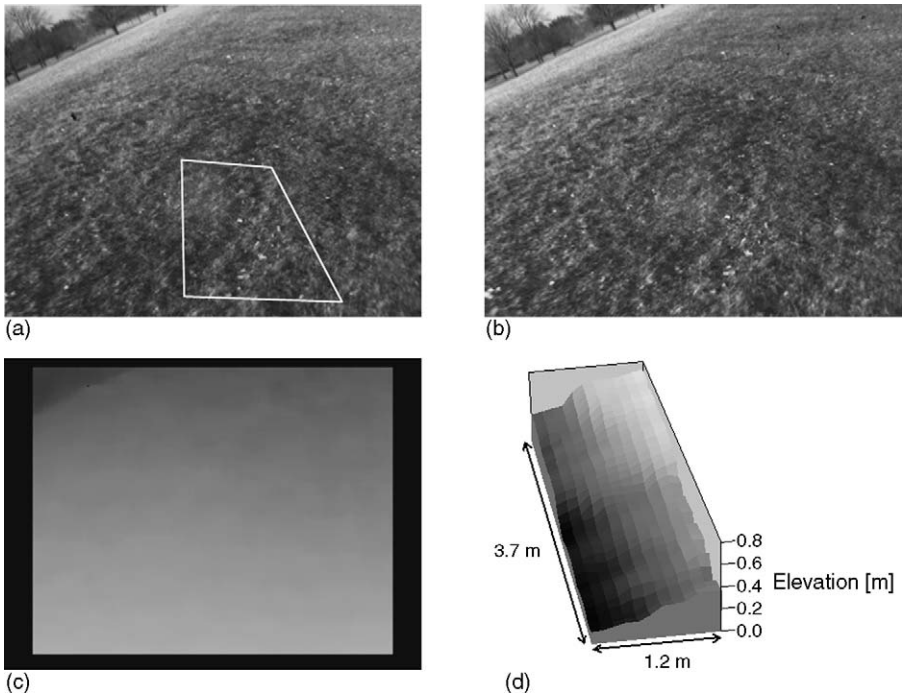

Fig. 6. Example of 3D terrain map creation; (a) original left image with a white quadrangle indicating the ROI of the terrain map; (b) original right image; (c) disparity image computed from the two original images; (d) 3D terrain map created based on the information of the disparity image.

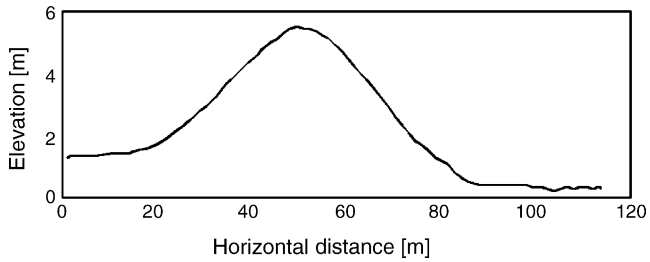

Fig. 7. Elevation at test site with a 6 m vertical difference.

traveled on the path shown in Fig. 7. Both the predicted and measured results indicate that the roll angle varies between -11° and 4° while traveling on the path. It can be seen that there is a constant offset between the predicted roll angle and the reference value at the same instant. Such offsets correspond to the look-ahead distance of the simulator: while the sensor provides the measured values at the position the vehicle is located, the simulator estimates the predicted

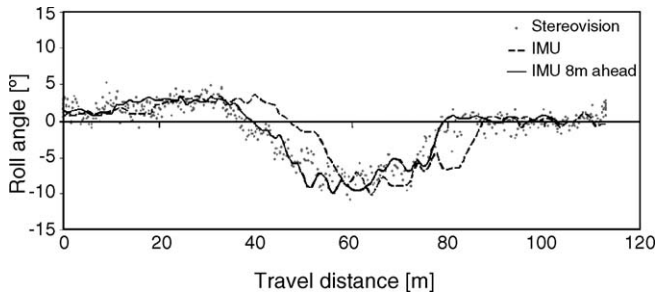

Fig. 8. predicted roll angle comparing to IMU data.

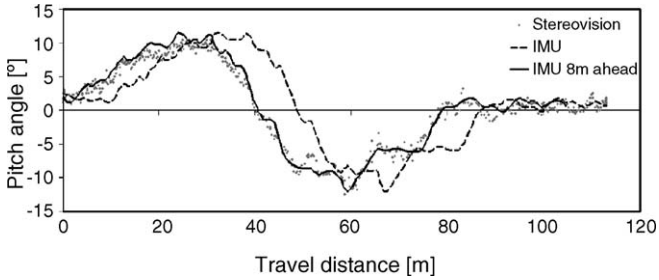

Fig. 9. Predicted pitch angle comparing to IMU data.

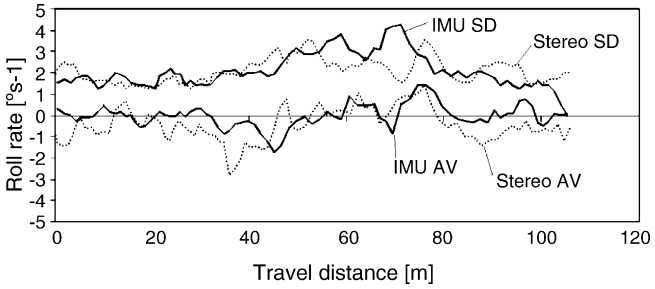

Fig. 10. Stochastic parameter of roll rate: S.D. and AV stand for standard deviation and average, respectively.

values about 8.0 m ahead of the current vehicle position. When shifting the IMU data 8.0 m ahead of the current vehicle position, the measured data fits the predicted data well. Such results show that the SIL motion simulator could accurately predict the vehicle roll angle 8.0 m ahead of the vehicle current position. The RMS error of the predicted roll angle referenced to the IMU data is less than 1.5° after shifting 8.0 m ahead.

Fig. 9 shows the comparison between the predicted pitch angles and the measured values on the same path. Similar to the result shown in Fig. 8, the motion simulator can accurately predict the pitch angle 8.0 m ahead of the moving vehicle. Both the predicted and the measured pitch angles vary between −12° and 12° on this test path. After realigning the predicted and measured pitch angels, the RMS error is less than 1.0°. Fig. 10 shows the comparison of the standard deviation and average value of the roll rate between the simulation results and the IMU measurements. The measured roll rate average and standard deviation are calculated based on a set of data obtained within the same window as the virtual vehicle traveling in the simulator (2.0 m), and are realigned by shifting 8.0 m ahead to make them comparable. The data analysis showed that the RMS errors between the measured and the predicted roll rates in the same window were 0.72° s^{-1} for the average value and 0.72° s^{-1} for the standard deviation. Similarly, for pitch rate in the same trial, the RMS errors were 1.10° s^{-1} for the average and 0.88° s^{-1} for the standard deviation, respectively. These results

Table 2
Result of the dynamic test at five different site: roll and pitch range represent minimum and maximum roll and pitch angle obtained during corresponding test; S.D. and AV stand for standard deviation and average, respectively

	Test site			Estimation error (RMS)					
Test no.	Roll angle (°)	Pitch range (°)	Vertical difference (m)	Roll (°)	Pitch (°)	Roll rate (S.D.) (° s^{-1})	Roll rate (AV) (° s^{-1})	Pitch rate (S.D.) (° s^{-1})	Pitch rate (AV) (° s^{-1})
1	−10 to 4	−12 to 12	5.3	1.5	1.1	0.72	0.72	0.88	1.10
2	−1 to 11	−8 to 14	5.2	2.1	1.3	0.93	0.59	1.00	1.24
3	−3 to 12	−10 to +5	5.3	1.8	1.1	0.97	0.67	0.81	1.16
4	−1 to 11	−4 to 6	3.2	1.5	1.0	0.86	0.53	0.83	1.03
5	−4 to 5	4 to 11	2.7	1.7	1.0	0.97	0.86	0.74	1.16
Average				1.7	1.1	0.89	0.67	0.85	1.14

indicate that the motion simulator can accurately reconstruct the stochastic parameters of the roll and pitch rates based on the SIL model.

The results obtained from all dynamic tests with different topographies are summarized in Table 2 (the results of test no. 1 are shown in Figs. 7–10). These results verify that the SIL vehicle attitude simulator can predict the look-ahead attitude and motion of the moving vehicle 8.0 m ahead of the current vehicle location with favorable and consistent accuracy at various field topographies.

4. Conclusion

This research investigated an innovative sensor-in-the-loop (SIL) simulator technology for assessing the tractor rollover possibility by estimating the vehicle motion status a few meters ahead of the vehicle actual position. This SIL simulator can covert the 3D field scene information obtained from a stereovision camera to create a virtual field terrain map. A virtual tractor will travel on the virtual field to assess the possibility of tractor rollover on the specific terrain. Static evaluation test results showed that 3D images acquired using the vehicle-mounted stereo camera could provide sufficient information to reconstruct artificial slopes of various attitudes with the RMS errors less than 1.4° for roll angle, and 2.2° for pitch angle, respectively. Field dynamic tests on a field with various slope topographies showed that the SIL simulator was capable of predicting both roll and pitch angles and roll and pitch angular rates of a moving vehicle 8.0 m ahead of the vehicle based on acquired stereo images with favorable and consistent accuracy.

The current SIL simulator has not yet taken into account when estimating tractor attitudes a few crucial factors of tractor operation, such as acceleration, turning radius and direction, and the attachment of an implement to the tractor. A further study will create a rollover risk index as a function of dynamically changing tractor attitude and motion parameters caused by the above-mentioned factors. This proposed rollover risk index will furnish the SIL simulator with the capability of a predictive tractor rollover prevention function, and therefore create active rollover protection technology for mobile agricultural machinery.

Acknowledgements

The material presented in this paper was based upon work supported partially by the Great Lakes Center for Agricultural Safety and Health (GLCASH) and USDA Hatch Funds (ILLU-10-352 AE). The Japan Society for the Promotion of Science (JSPS) provides a Fellowship Fund to support Dr. Michio Kise's postdoctoral research at the University of Illinois at Urbana-Champaign. Any opinions, findings, and conclusions expressed in this publication are those of the authors and do not necessarily reflect the views of the University of Illinois, GLCASH, JSPS and USDA.

References

ASAE, 1997. ASAE standards: roll-over protective structures (ROPS) for wheeled agricultural tractors (ISO compatible). ASAE S519 DEC94.

Beggs, J.S., 1983. Kinematics. Hemisphere Publishing Corp., Washington, DC.

Etherton, J.R., Cutlip, R.G., Harris, J.R., Ronaghi, M., Means, K.H., Howard, S., 2002a. Dynamic performance of the mechanism of an automatically deployable ROPS. J. Agric. Safety Health 8 (1), 113–118.

Etherton, J.R., Cutlip, R.G., Harris, J.R., Ronaghi, M., Means, K.H., Gillispie, A., 2002b. Static load test performance of a telescoping structure for an automatically deployable ROPS. J. Agric. Safety Health 8 (1), 119–126.

Davis, D.C., Rehkugler, G.E., 1974a. Agricultural wheel-tractor overturns. Part I. Mathematical model. Trans. ASAE 17 (3), 477–483.

Davis, D.C., Rehkugler, G.E., 1974b. Agricultural wheel-tractor overturns. Part II. Mathematical model verification by scale-model study. Trans. ASAE 17 (3), 484–488.

Hard, D.L., Myers, J.R., Snyder, K.A., Casini, V.J., Morton, L.L., Cianfrocco, R., Fields, J., 1999. Identifying work-related fatalities in the agricultural production sector using two national occupational fatality surveillance systems, 1990–1995. J. Agric. Safety Health 5 (2), 155–169.

He, D.X., Matsuura, Y., Kozai, T., Ting, K.C., 2003. A binocular stereovision system for transplant growth variables analysis. Appl. Eng. Agric. 19 (5), 611–617.

Kise, M., Zhang, Q., Rovira Más, F., 2005. A Stereovision-based crop row detection method for tractor-automated guidance. Biosyst. Eng. 90 (4), 357–367.

Lines, J.A., Tillett, R.D., Ross, G.L., Chan, D., Hockaday, S., McFarlane, N.J.B., 2001. An automatic image-based system for estimating the mass of free-swimming fish. Comput. Electron. Agric. 31 (2), 151–168.

Liu, J., Ayers, P.D., 1998. Application of a tractor stability index for protective structure deployment. J. Agric. Safety Health (1), 171–181 (Special issue).

Liu, J., Ayers, P.D., 1999. Off-road vehicle rollover and filed testing of stability index. J. Agric. Safety Health 5 (1), 59–71.

Myers, J.R., Snyder, K.A., Hard, D.L., Casini, V.J., Cianfrocco, R., Fields, J., Morton, L., 1998. Statistics and epidemiology of tractor fatalities—a historical perspective. J. Agric. Safety Health 4 (2), 95–108.

National Safety Council, 1999. Accident Facts. National Safety Council, Chicago, IL.

Personick, M., Windau, J., 1997. Self-employed Individuals Fatally Injured at Work. United States Bureau of Labor Statistics, Washington, DC, pp. 55–62.

Powers, J.R., Harris, J.R., Etherton, J.R., Snyder, K.A., Ronaghi, M., Newbraugh, B.H., 2001. Performance of an automatically deployable ROPS on ASAE tests. J. Agric. Safety Health 7 (1), 51–61.

Rautiainen, R.H., Reynolds, S.J., 2002. Mortality and morbidity in agriculture in the United States. J. Agric. Safety Health 8 (3), 259–276.

Reid, J.F., Searcy, S.W., 1987. Vision-based guidance of an agricultural tractor. IEEE Control Syst. Mag. 7 (12), 39–43.

Rovira Más, F., Zhang, Q., Reid, J.F., 2005. Creation of three-dimensional crop maps based on aerial stereo images. Biosyst. Eng. 90 (3), 251–259.

Scharstein, D., 1999. View Synthesis Using Stereovision. Lecture Note in Computer Science. Springer-Verlag, Berlin.

Spencer, H.B., Gilfillan, G., 1976. An approach to the assessment of tractor stability on rough slope ground. J. Agric. Eng. 21 (2), 169–176.

Wilkins III, J.R., Engelhard, H.L., Bean, T.L., Byers, M.V., Crawford, J.M., 2003. Prevalence of ROPS-equipped tractors and farm/farmer characteristics. J. Agric. Safety Health 9 (2), 107–118.

Wu, J., Tillett, R., McFarlane, N., Ju, X., Siebert, J.P., Schofield, P., 2004. Extracting the three-dimensional shape of live pigs using stereo photogrammetry. Comput. Electron. Agric. 44 (3), 203–222.

Yakowitz, S., Szidarovszky, F., 1989. An Introduction to Numerical Computations. Macmillan, New York.